

LS-DYNA MAT54 modeling of the axial crushing of a composite tape sinusoidal specimen

Paolo Feraboli^{a,*}, Bonnie Wade^a, Francesco Deleo^a, Mostafa Rassaian^b, Mark Higgins^b, Alan Byar^b

^aAutomobili Lamborghini Advanced Composite Structures Laboratory, Dept. of Aeronautics & Astronautics, University of Washington, Seattle, WA 98195-2400, United States

^bCrashworthiness and Impact Survivability, Applied Structural Methods, Boeing Research & Technology, Seattle, WA, United States

ARTICLE INFO

Article history:

Received 30 April 2011

Received in revised form 30 July 2011

Accepted 8 August 2011

Available online 16 August 2011

Keywords:

Crashworthiness

A. Carbon fiber

B. Impact behavior

C. FEA

ABSTRACT

The suitability of a progressive failure material model to simulate the quasi-static crushing of a composite specimen is evaluated. The commercially available material model MAT54 “Enhanced Composite Damage” in LS-DYNA is often utilized to simulate damage progression in dynamic failure simulations because it requires a reduced number of experimental input parameters compared to damage mechanics-based material models. The composite specimen used for the experiments is a semi-circular sinusoid, and is comprised of carbon fiber/epoxy unidirectional prepreg tape. Results show that MAT54 can successfully reproduce experimental results, however the simulation is highly sensitive to changes in model parameters, which are either non-physical (i.e. are purely mathematical expedients), or cannot be measured experimentally. These include element size, contact definition, load–penetration curve, and crush front softening parameter, among others. Therefore, achieving successful simulation results requires extensive calibration of these parameters by trial and error, and a deep understanding of the strengths and challenges of the selected modeling strategy.

© 2011 Elsevier Ltd. All rights reserved.

1. Introduction

The behavior of composite materials under crash conditions poses particular challenges for engineering analysis since it requires modeling beyond the elastic region and into failure initiation and propagation. Crushing is the result of a combination of several failure mechanisms, such as matrix cracking and splitting, delamination, fiber tensile fracture and compressive kinking, frond formation and bending, and friction [1,2]. With today’s computational power it is not possible to capture all of these failure mechanisms in a single analysis. Models based on lamina-level failure criteria have been used, although with well-accepted limitations [3], to predict the onset of damage within laminate codes. Once failure initiates, the mechanisms of failure propagation require reducing the material properties using several degradation schemes [4]. To perform dynamic impact analysis, such as crash analysis, it is necessary to utilize an explicit finite element code, which solves the equations of motion numerically by direct integration using explicit rather than standard methods, for example using the central difference method [4]. Commercially available codes used for mainstream crash simulations include LS-DYNA, ABAQUS Explicit, RADIOSS and PAM-CRASH [5]. In general, these

codes offer built-in material models for composites. Each material model utilizes a different modeling strategy, which includes failure criterion, degradation scheme, material properties, and usually a set of model-specific input parameters that are typically needed for the computation but do not have an immediate physical meaning. Composites are modeled as orthotropic linear elastic materials within the failure surface, whose shape depends on the failure criterion adopted in the model [4]. Beyond the failure surface, the appropriate elastic properties are degraded according to degradation laws. Depending upon the specific degradation law used, the constitutive models can be divided into either progressive failure models (PFM) or continuum damage mechanics models (CDM). The commercial software package LS-DYNA [6] offers a variety of material models for composite materials, which include both PFM (MAT22 and MAT54/55) and CDM (MAT58 and MAT162). The failure criteria for laminated composites in PFM are typically strength-based, and use a ply discount method to degrade material properties. At the failure surface, the values of the appropriate elastic properties of the ply in the material direction are degraded from the undamaged state, which is 1, to the fully damaged state, which is typically 0. The material model stress–strain curve does not require that a specific unloading/softening curve be assigned, and after the strength of the ply is exceeded the properties are immediately dropped to zero. The so-called progressive failure is realized through ply-by-ply failure within the laminate, and once all plies have failed the element is deleted [6].

* Corresponding author. Tel.: +1 011 206 543 2170; fax: +1 011 206 543 0217.

E-mail address: feraboli@aa.washington.edu (P. Feraboli).

In this paper, the quasi-static energy absorption achieved through crushing of a composite specimen, consisting of a semi-circular sinusoid and manufactured with carbon fiber/epoxy unidirectional prepreg tape, is modeled using the PFM material model MAT54 in LS-DYNA. Details of the specimen design, manufacturing, and testing procedure have been previously published by the authors in [7]. The sinusoidal geometry is desirable from a modeling standpoint because it is self-stabilizing, i.e. it does not require potting or a support fixture to prevent buckling during crushing, as does a flat plate specimen [8], and because it does not have hoop-fiber constraint, such as a tubular specimen [2,9]. The focus of the discussion is centered on the analysis approach, and the sensitivity of the model to parametric variations. Results show that while MAT54 can be used to successfully simulate the experiment, the modeling strategy is not truly predictive and several modeling parameters need to be calibrated by trial and error.

2. Experiment

Specimens are manufactured by press-molding through a set of aluminum matching tools, and details are given in [7]. The sinusoidal specimen features a semicircular segment, of radius 6.4 mm (0.25 in.), repeated three times at alternating sides with respect to the midplane, Fig. 1a. The material system is T700 carbon fiber/2510 epoxy prepreg, supplied by Toray Composites of America. It is a unidirectional tape 12 k tow, and a 270° F cure resin (132 °C) designated for autoclave or oven-only cure. The lay-up is $[0/90]_{3s}$, yielding an average cured laminate thickness of 0.079 in.

(2.0 mm). This material is used extensively for General Aviation primary structures, and its properties are well documented as part of the FAA-sponsored AGATE Program (Advanced General Aviation Transport Experiment) [10,11]. A summary of the material properties is provided in Table 1. The upper end of the corrugated specimen is machined with a single-sided 45° chamfer to favor the initiation of stable crushing at the chosen end of the specimen, and to avoid undesired initial spikes in crush loads which may lead to specimen instability [7]. This chamfer is known as the trigger, or crush initiator, and is shown in Fig. 1b. Specimens are tested in the vertical configuration, resting on a polished hardened steel surface, at a crosshead velocity of 1 in./min (25.4 mm/min.). Seven repetitions are used to obtain average data. Fig. 2a–c shows typical curves for a single test, in the following order: the load curve (a), the specific energy absorption (b), and the total energy absorbed (c) as a function of displacement. The definitions of the specific energy absorption (SEA) and total energy absorbed (EA) are given in [7]. For the following analysis section, the entire load–displacement curve [12] of Fig. 2a (initial slope, peak load, and average crush load) and the average SEA value of Fig. 2c (SEA = 67.06 J/g) are used as benchmarks for comparing the success of the simulation results.

3. Description of the MAT54 material model and other model input parameters

MAT54 is designed specifically to handle orthotropic materials such as unidirectional tape composite laminates (not fabric).

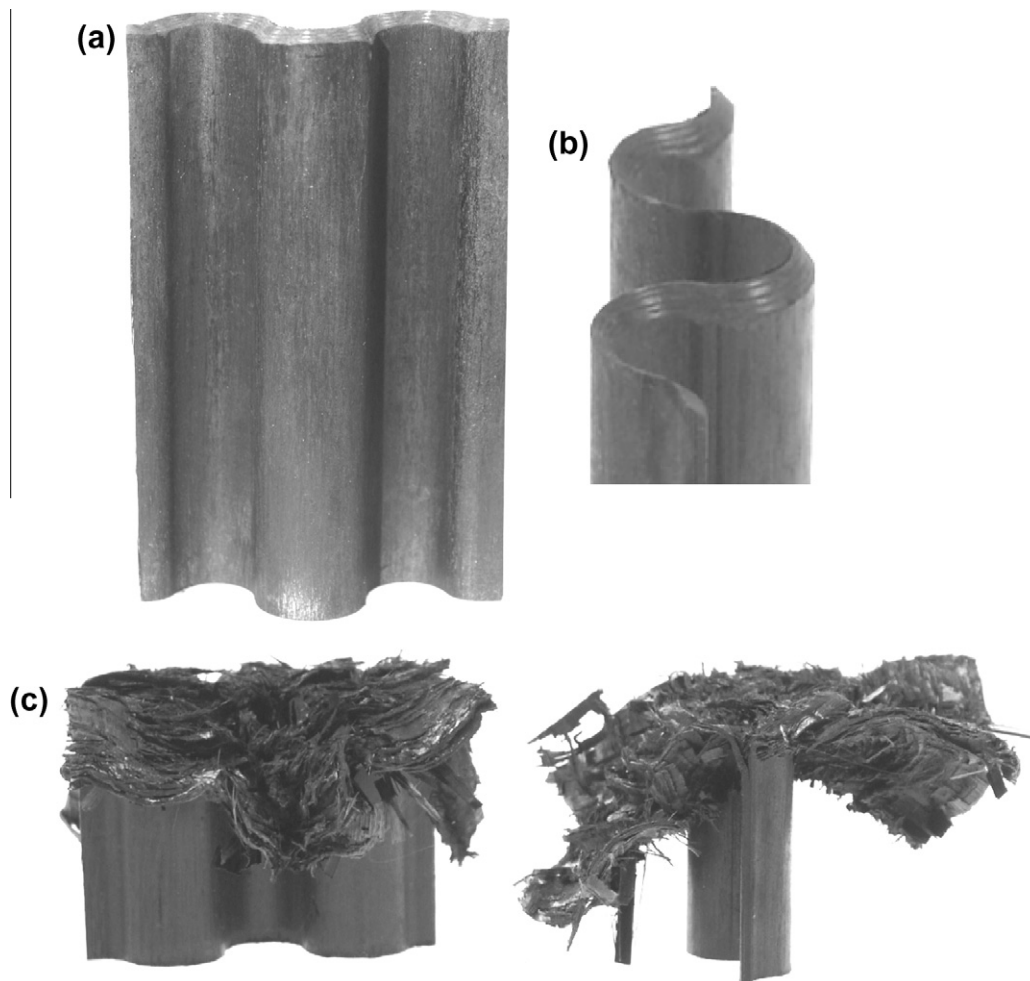


Fig. 1. Prepreg tape corrugated specimen (a), detail of the chamfered trigger (b), and typical morphology after crush testing (c).

Table 1
Material properties of T700/2510 Unidirectional tape as published in the CMH-17 [10,11].

Property	Symbol	LS-DYNA parameter	Experimental value
Density	ρ	RO	0.055 lb/in. ³ (1.52 g/cm ³)
Modulus in 1-direction	E_1	EA	18.4 Msi (127 GPa)
Modulus in 2-direction	E_2	EB	1.22 Msi (8.41 GPa)
Shear modulus	G_{12}	GAB	0.61 Msi (4.21 GPa)
Major Poisson's ratio	ν_{12}	–	0.309
Minor Poisson's ratio	ν_{21}	PRBA	0.02049
Strength in 1-direction, tension	F_1^{tu}	XT	319 ksi (2.20 GPa)
Strength in 2-direction, tension	F_2^{tu}	YT	7.09 ksi (48.9 MPa)
Strength in 1-direction, compression	F_1^{cu}	XC	213 ksi (1.47 GPa)
Strength in 2-direction, compression	F_2^{cu}	YC	28.8 ksi (199 MPa)
Shear strength	F_{12}^{su}	SC	22.4 ksi (154 MPa)

Unfortunately, the LS-DYNA theory/user manual [6] does not contain detailed definitions of the input parameters used, so it is important to provide them here, see Table 2.

In the elastic region, the material stress–strain curves in MAT54 for the fiber (1-direction), matrix (2-direction) and shear (1–2 direction) are given by:

$$\varepsilon_1 = \frac{1}{E_1} (\sigma_1 - \nu_{12} \sigma_2) \quad (1)$$

$$\varepsilon_2 = \frac{1}{E_2} (\sigma_2 - \nu_{21} \sigma_1) \quad (2)$$

$$2\varepsilon_{12} = \frac{1}{G_{12}} \tau_{12} + \sigma \tau_{12}^3 \quad (3)$$

In Eq. (3), the α (ALPH in Table 2) input parameter is a weighing factor for the nonlinear shear stress term. ALPH cannot be measured experimentally but needs to be calibrated by trial and error. Beyond the elastic region, MAT54 uses the Chang-Chang failure criterion [6,13] to determine individual ply failure as shown in Eqs. (4)–(7). In the following equations: *ef*, *ec*, *em* and *ed* are called history variables and they represent (respectively) tension and compression for the 1-direction and tension and compression for the 2-direction. XT is the fiber tensile strength, XC is the fiber compressive strength, YT is the matrix tensile strength, YC is the matrix compressive strength, and SC is the shear strength of the unidirectional ply. These input parameters can be measured through testing of the unidirectional tape lamina. It should be noted that all of these quantities assume that the 1-direction is the fiber direction, while the 2-direction is the matrix direction. For this reason, all calculations in MAT54 assume that the material is unidirectional tape, and not fabric, where otherwise both the 1- and 2-directions would be fiber directions. The only difference between MAT54 and MAT55 is that the latter uses the Tsai-Wu failure criterion.

For the tensile fiber mode where $\sigma_{11} \geq 0$:

$$e_f^2 = \left(\frac{\sigma_{11}}{F_1^{tu}} \right)^2 + \beta \left(\frac{\sigma_{12}}{F_{12}^{su}} \right)^2 \quad \begin{cases} \geq 1 \text{ failed} \\ < 1 \text{ elastic} \end{cases} \quad (4)$$

Upon failure: $E_1 = E_2 = G_{12} = \nu_{12} = \nu_{21} = 0$.

The MAT54 shear stress weighing factor β (BETA in Table 2) allows the user to explicitly define the influence of shear in the tensile fiber failure mode. For BETA = 1 the Hashin [6] failure criterion is implemented, while setting BETA = 0 reduces Eq. (4) to the Maximum Stress failure criterion. Selecting the right value of BETA

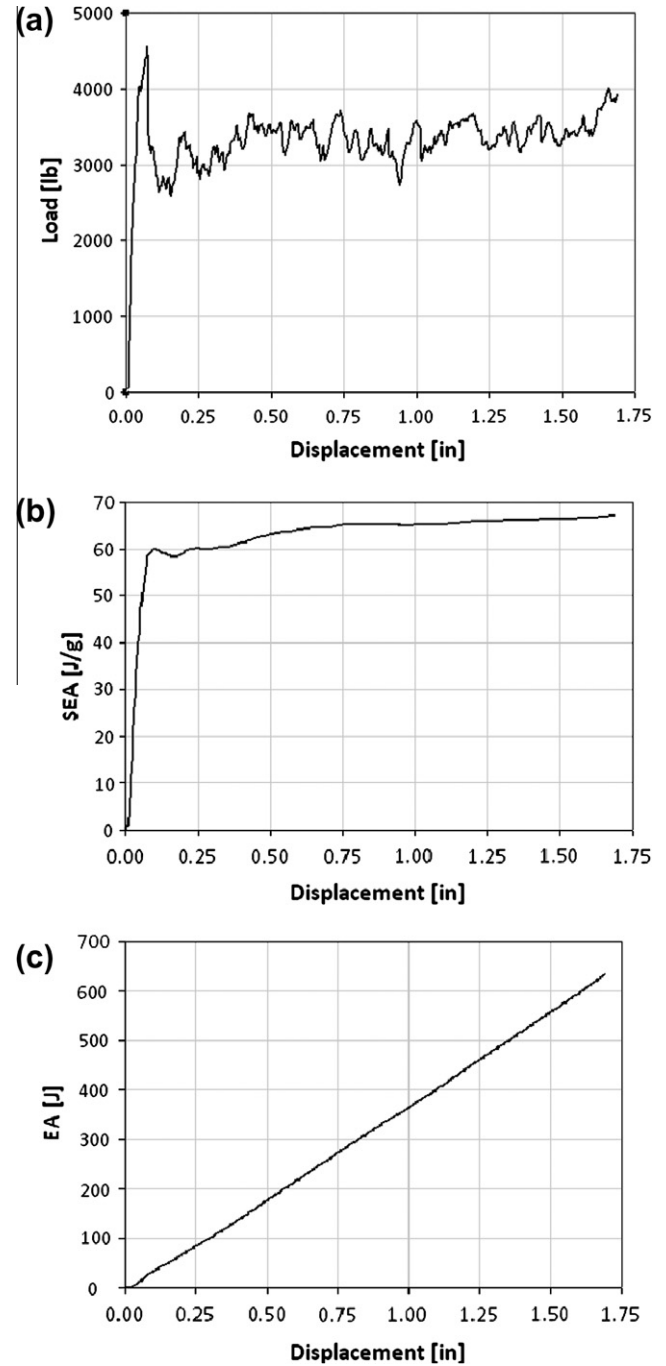


Fig. 2. Experimental load–displacement curve (a), specific energy absorption (b), and total energy absorbed (c) as a function of displacement.

is a matter of preference, and otherwise can be done by trial and error.

For the compressive fiber mode where $\sigma_{11} \leq 0$:

$$e_c^2 = \left(\frac{\sigma_{11}}{F_1^{cu}} \right)^2 \quad \begin{cases} \geq 1 \text{ failed} \\ < 1 \text{ elastic} \end{cases} \quad (5)$$

Upon failure: $E_1 = \nu_{12} = \nu_{21} = 0$.

For the tensile matrix mode where $\sigma_{22} \geq 0$:

$$e_m^2 = \left(\frac{\sigma_{22}}{F_2^{tu}} \right)^2 + \left(\frac{\sigma_{12}}{F_{12}^{su}} \right)^2 \quad \begin{cases} \geq 1 \text{ failed} \\ < 1 \text{ elastic} \end{cases} \quad (6)$$

Upon failure: $E_2 = \nu_{21} = G_{12} = 0$.

For the compressive matrix mode where $\sigma_{22} \leq 0$:

$$e_d^2 = \left(\frac{\sigma_{22}}{2F_{12}^{su}} \right)^2 + \left[\left(\frac{F_2^{cu}}{2F_{12}^{su}} \right) - 1 \right] \frac{\sigma_{22}}{F_2^{cu}} \left(\frac{\sigma_{12}}{F_{12}^{su}} \right)^2 \quad \begin{cases} \geq 1 \text{ failed} \\ < 1 \text{ elastic} \end{cases} \quad (7)$$

Upon failure: $E_2 = \nu_{21} = \nu_{12} = 0 = G_{12} = 0$.

When one of the above conditions is exceeded in a ply within the element, all specified elastic properties of that ply are set to zero. Matrix failure corresponds to first ply failure. The FBRT and YCFAC strength reduction parameters in Table 2 are used to degrade the pristine fiber strengths of the remaining plies once matrix failure takes place. This strength degradation is applied using the following equations:

$$XT = XT^* * FBRT \quad (8)$$

$$XC = YC^* * YCFAC \quad (9)$$

The FBRT factor acts as a percentage reduction of the tensile fiber strength from its pristine value, therefore its value may only be in the range [0, 1]. The YCFAC factor uses the pristine matrix strength YC to determine the damaged compressive fiber strength, which means that the upper value of YCFAC is not 1 but $XC/YC = 7.4$. The input value for the two parameters FBRT and YCFAC cannot be measured experimentally and need to be determined by trial and error.

In addition to these strength-based criteria, failure can also occur if the strains exceed the strain-to-failure for each ply. For a unidirectional tape, the DFAILT and DFAILC parameters are the tensile and compressive failure strains in the fiber direction, while DFAILM is the failure strain in the matrix direction. By definition, DFAILT must be positive and DFAILC must be negative. If DFAILT, DFAILC or DFAILM are set to zero, the code ignores the parameters altogether and failure can only occur by the Chang-Chang failure criterion. If DFAILT, DFAILC and DFAILM are non-zero, failure can occur if one of the strains exceeds the strain-to-failure. An additional strain-to-failure, DFAILS for shear, is used in the code but it does not appear as a criterion for failure. This means that if the shear strain exceeds the assigned value of DFAILS, failure does not occur. All strains-to-failure can be measured through coupon-level tests of the unidirectional lamina, however if they are not known LS-DYNA gives the user the possibility to employ a generic parameter EFS (effective failure strain). If EFS is greater than zero, failure occurs if the effective strain is greater than EFS. If EFS is set to zero, the parameter is ignored. This parameter is not truly a physical property, and can only be estimated by trial and error.

Element deletion can also occur if the element time step TFAL is exceeded. The value of TFAL determines whether or not the simulation considers a minimum time step for element deletion, and what that minimum time step is. This option is useful only in cases where the computational cost of the simulation is driven up by highly distorted elements that no longer carry load but do not fail from the prescribed element deletion criterion. It is necessary that these costly elements have very small time steps to handle the high degree of distortion. By defining a minimum allowed time step using TFAL, these costly but useless distorted elements can be eliminated. TFAL is defined as follows:

$TFAL \leq 0$: No element deletion by time step size

$0 < TFAL \leq 0.1$: Element is deleted when its time step is smaller than TFAL

$TFAL > 1$: Element is deleted when $\frac{\text{current time step}}{\text{original time step}} < TFAL$

For crush simulations, only positive nonzero values can be implemented since for $TFAL = 0$ the crush front parameter SOFT is deactivated ($SOFT = 1$).

Lastly, the SOFT parameter, or crush front reduction factor, is a mathematical expedient used to reduce the strength of the elements immediately ahead of the crush front, i.e. the row of elements that will be loaded once the current row is deleted. This parameter is used to avoid instability and to ensure stable crushing when the load transitions from the active row of elements to the next. Approaching failure, the load reaches its peak in the active row of elements, and at failure it is suddenly dropped to zero. If the SOFT parameter is set to zero (hence made inactive), this sudden transition may lead to unstable buckling of the section. In order to be active, the value of the SOFT parameter must be defined within the range [0, 1], where $SOFT = 1$ indicates that elements at the crush front retain their pristine strength and no softening takes place. For SOFT values near zero, the strength is nearly completely reduced. SOFT values greater than unity deactivate the parameter, and the model acts as if SOFT is zero. Since this parameter cannot be measured experimentally, it needs to be calibrated by trial and error.

4. Description of the baseline MAT54 model

The LS-DYNA model is represented in Fig. 3 and shows the loading plate, the composite specimen and the trigger row. The geometry is imported into LS-DYNA and meshed using a fully integrated linear shell element (formulation 16) of 0.1 in. \times 0.1 in. (2.54 mm \times 2.54 mm) square element size. Since the laminate thickness is 0.079 in. (2.0 mm), the aspect ratio of the element is $0.079/0.1 = 0.79$.

For the 12-ply corrugated specimen, there are 12 integration points ($NIP = 12$ in the LS-DYNA shell element definition). Each ply is defined by 1 integration point through the thickness, with the prescribed orientation. The specimen is modeled with a total of 840 elements, having constant thickness of 0.079 in. (2.0 mm). The material stress–strain curves in the fiber (1) and matrix (2)

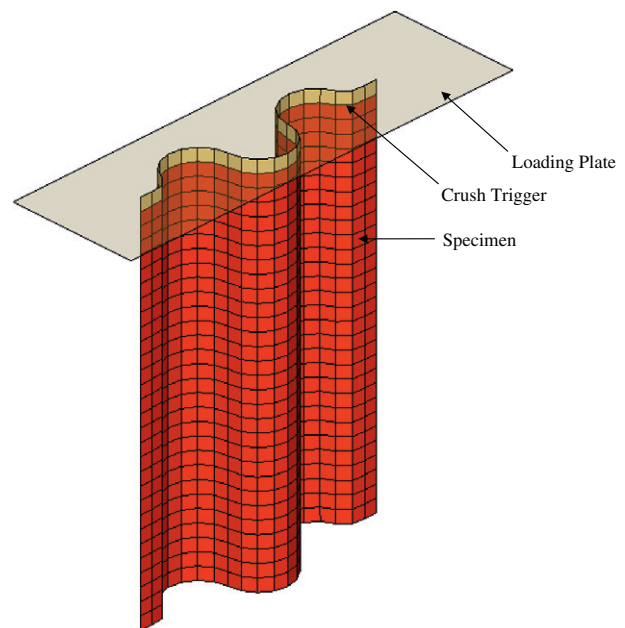


Fig. 3. LS-DYNA model of the corrugated composite specimen, crush trigger, and loading plate. (For interpretation of the references to colour in this figure legend, the reader is referred to the web version of this article.)

directions are used as input parameters for the MAT54 material card. These curves are generated using the values of Table 1, and are shown in Fig. 4a and b. It should be noted that the shape and the magnitude of the two curves are different. For English units, the material density input RO must be converted from pound-weight to pound-mass by dividing by a gravity factor of 386.4 (in./s²). The value of 0.05 lbf/in.³ (1.52 g/cm³) is input into MAT54 as 0.05/386.4 = 0.15E-3 lbm/in.³. The input deck for the baseline MAT54 material model is given in Table 3. The meaning of all parameters, including the inactive ones that are indicated with a strikethrough, is given in Table 2.

The trigger is modeled as a single row of reduced thickness (0.01 in. or 0.25 mm) elements at the crush front of the specimen. In order to apply different element properties to the trigger row such as the element thickness, the trigger must be modeled as a separate part from the corrugated coupon. The trigger is then merged to the rest of the specimen in a part set, and the two parts act as one. The specimen is kept at rest by constraining all degrees of freedom using a nodal single point constraint (SPC) boundary condition on the bottom row of nodes opposite the crush trigger. A large single shell element perpendicular to the specimen crush front is used to model the loading plate.

A contact definition between the loading plate and the specimen is necessary for the two parts to properly interact. LS-DYNA offers a variety of built-in contact algorithms, which can be divided in three categories: the kinematic constraint method for contact and release, the penalty method for prolonged contact, and the distributed parameter method for sliding contact. For crash analysis, standard penalty formulation methods are used [14,15]. These

methods place springs normal to the surface between all penetrating nodes and the contact surface in order to facilitate a reaction force upon contact. The stiffness of the springs is determined directly from the value of the penalty stiffness parameter used by the specific contact algorithm. The reaction force due to contact is a function of the normal distance between two parts multiplied by a constant penalty factor, which acts as the spring stiffness constant. It is common practice to employ a continuous load-penetration (LP) curve rather than a single constant penalty factor. This curve defines the reaction normal force applied to each node as a function of the distance the node has penetrated through the surface that it is contacting. The LP curve influences the initial slope of the numeric crush curve, as well as the overall stability of the simulation since it dictates how gradually the load is introduced into the row of elements at the crush front. The LP curve constitutes the most critical characteristic for a given contact type. Further discussion will be given in the parametric analysis section that follows. The contact interface between the loading plate and the specimen is defined using the contact type “Entity” for the baseline simulation. This contact type is relatively simple to implement since it requires a reduced set of parameter definitions relative to other standard penalty formulation contact types, and it produces stable results. The master part for Entity is a rigid body geometry, the loading plate in this case. Three alternative contact types have been attempted: “Rigid Nodes to Rigid Body”, “Eroding Surface to Surface”, and “Automatic Surface to Surface”. Good results can also be obtained using the “Rigid Nodes to Rigid Body” contact type, but the different contact type will be evaluated in a separate publication. The other two contact types, “Eroding Surface to Surface” and “Automatic Surface to Surface”, do not work well for this kind of load-specimen configuration. As soon as a row of elements comes into contact with the loading plate, it generates a sharp impulse load, which immediately deletes the element row. This peak is followed by zero load until the next row is loaded, thus preventing the load to ever achieve a stable crush value.

Typically, contact type Entity defines a virtual geometry as the master part in the contact. For the crush coupon simulation however, there is a physical geometry that contacts the specimen; hence the master part is the loading plate itself. Meshing of the master part may only be made with a shell mesh within the contact type Entity; therefore the element formulation for the loading plate is the default shell element formulation for explicit calculations (formulation 2), with two integration points through the thickness. The material system of the loading plate is defined using the rigid body material model MAT20, which attributes non-deformable characteristics to the plate, with steel material properties. The plate has a thickness of 0.3 in. (7.6 mm), and in-plane dimensions 4 in. × 1 in. (101.6 mm × 25.4 mm). The density is assigned to be 0.283 lb/in.³ (7.83 g/cm³) and the total mass is 0.34 lb (154 g).

Solution time takes 96 s using a workstation with a 2.26 GHz dual Quadcore (8 processors) 64-bit 16 GB RAM computer. The velocity of the plate is 150 in./s (3.81 m/s), and is defined by a linear load curve imposed on the nodes of the loading plate. The effect of using a simulation crush velocity that is much higher than the experimental one is discussed in the following section.

The time progression of the baseline simulation, Fig. 5, reveals that failure advances in an even and stable fashion, through element deletion at the crush front. When the first ply in an element fails, the element remains in the straight position and does not exhibit a different morphology. Once all plies have failed, the element is immediately deleted. Once an element is deleted, the entire row of elements is also deleted. Therefore crush progresses with a progressive deletion of the crush front row of elements without any other graphic indication. It is an unfortunate characteristic of MAT54 that it does not allow elements to form fronds that mimic

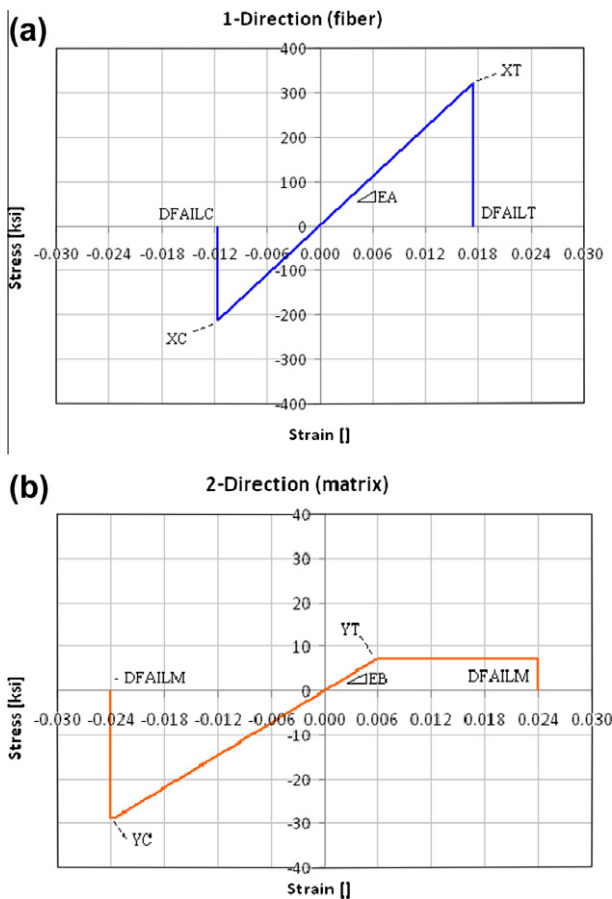


Fig. 4. Stress–strain curve for the material model MAT54 based on the experimental values of Table 1. (For interpretation of the references to colour in this figure legend, the reader is referred to the web version of this article.)

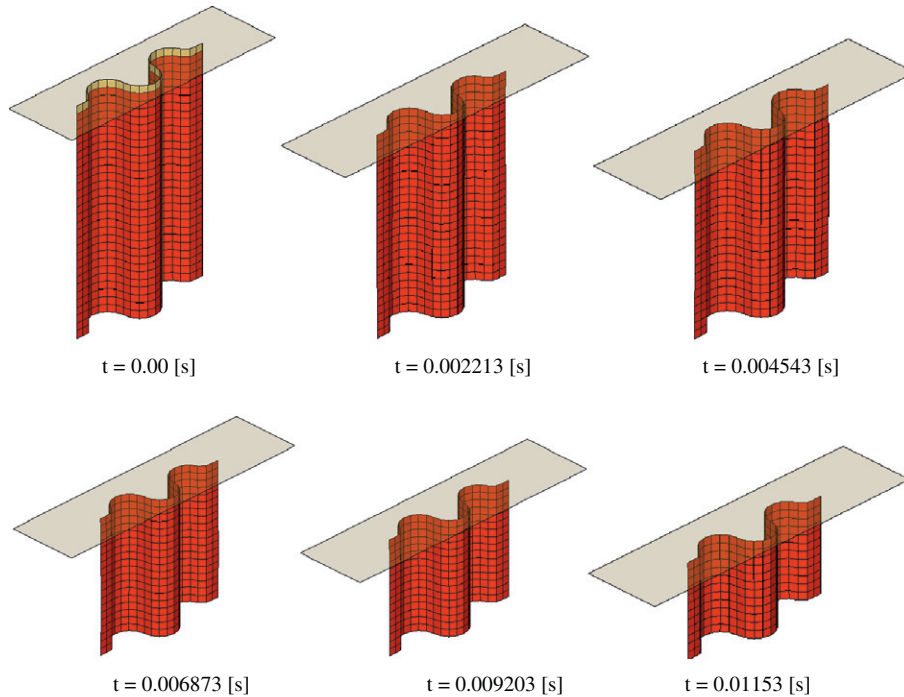


Fig. 5. Time progression of the baseline simulation showing stable element row deletion. (For interpretation of the references to colour in this figure legend, the reader is referred to the web version of this article.)

what actually happens in the physical world (Fig. 1c). It should be noted that this is a peculiar behavior of axial crush simulations, which are governed by the SOFT crush front parameter. Other simulations [14] have shown that MAT54 can exhibit a limited degree of damage morphology if not loaded in the axial direction, as in the case of flexure loading or through-thickness indentation of a flat plate.

The load–displacement curve obtained from the model is shown in Fig. 6 in its raw and filtered state. The raw curve is characterized by an alternating series of sharp peaks and valleys, giving it a saw tooth appearance. This feature is a typical result of the mathematical model, which exhibits linear loading up to failure at the peak, then the load drops to zero upon deletion of the current row of elements, until the next row of elements picks up the load again. It is common practice to filter the numeric results using a low-pass digital filter (SAE 600 Hz) during post-processing

[4,5,15]. Through filtering, the average crush load remains unchanged, but the peaks and valleys are smoothed, Fig. 6. The curve oscillates about the average crush load without large variations in local peak values, indicating that the simulation is stable. The filtered crush curve from the baseline simulation is compared with the experimental curve in Fig. 7. The simulation captures all key characteristics of the experimental curve: initial slope, peak load, and average crush load, which in turn is used to compare the SEA value of the simulation to the experimentally measured SEA value. The predicted value is 64.12 J/g, compared to the experimental 67.06 J/g, the difference being –4.4%.

In this section it was shown how material model MAT54 can be used to generate a model that closely approximates the experiment and captures all of its significant features. In the following two sections the sensitivity of the model to variations in the MAT54 input parameters is investigated. As summarized in

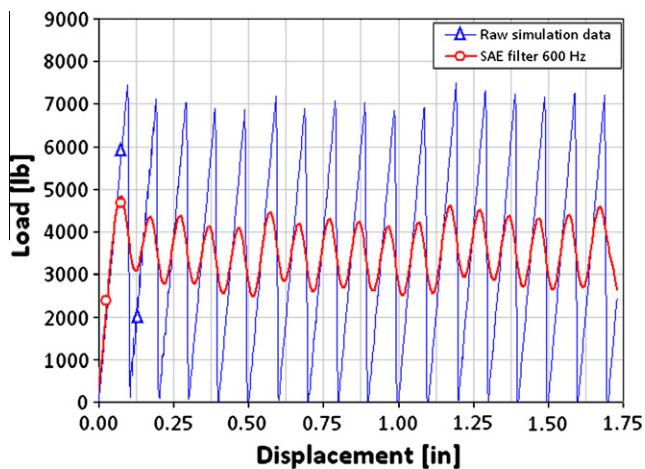


Fig. 6. Filtered versus raw numeric crush data from the baseline simulation. (For interpretation of the references to colour in this figure legend, the reader is referred to the web version of this article.)

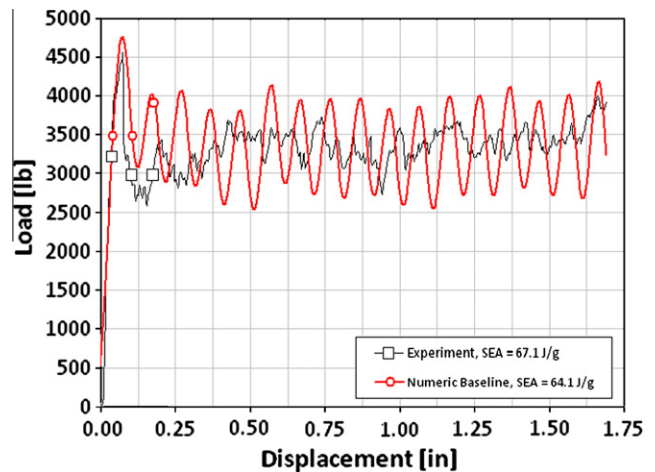


Fig. 7. Experimental and model baseline load–displacement curves. (For interpretation of the references to colour in this figure legend, the reader is referred to the web version of this article.)

Tables 2 and 3, the material card for MAT54 contains input parameters for both material properties and other code-specific parameters. Material properties include physical properties (density), elastic properties (moduli and Poisson’s ratios), and failure properties (strengths and strains to failure). Other code-specific parameters include failure criterion parameters (ALPHA, BETA and CRIT), degradation scheme factors (FBRT and YCFAC), geometrical features (AOPT, MANGLE, etc.), and other non-physical parameters that are required for the simulation to run (SOFT and TFAIL). A summary of the parameters varied and their value is reported in Table 4, which also lists the corresponding figure in the text.

5. Sensitivity of the MAT54 material model to material properties

An effective model needs to be sufficiently robust to tolerate small variations in material property input data, in order to

Table 2
MAT54 input parameter definitions.

Variable	Definition	Suggested value
MID	Material identification number	Any arbitrary integer
RO	Mass per unit volume [*]	ρ From material properties
EA	Young’s modulus in longitudinal direction	E_1 , from material properties
EB	Young’s modulus in transverse direction	E_2 , from material properties
PRBA	Minor Poisson’s ratio, $\nu_{ba} = \nu_{21}$	Calculated using ν_{12} , E_1 and E_2
PRCA	Minor Poisson’s ratio, $\nu_{ca} = \nu_{31}$	Not used
PRCB	Minor Poisson’s ratio, $\nu_{cb} = \nu_{32}$	Not used
GAB	Shear modulus, G_{ab}	G_{12} , from material properties
GBC	Shear modulus, G_{bc}	Assumed equal to G_{ab}
GCA	Shear modulus, G_{ca}	Assumed equal to G_{ab}
KF	Bulk modulus of material	Not used
AOPT	Material axes option parameter	AOPT = 3
A1 A2 A3	Vector components to define material axes for aopt = 2	Not used
MANGLE	Material angle in degrees used when aopt = 3	90°
V1 V2 V3	Vector components to define the material axes for aopt = 3	Unit vector in z direction: $v_1 = 0, v_2 = 0, v_3 = 1$
DFAILT	Max strain for fiber tension	Calculated using E_1 and F_1^{tu}
DFAILC	Max strain for fiber compression	Calculated using E_1 and F_1^{cu}
D1 D2 D3	Vector components to define the material axes for aopt = 2	Not used
DFAILM	Max strain for matrix straining in tension and compression	Greater than or equal to the maximum value of (YT/EB) or (YC/EB)
DFAILS	Max shear strain	$0 < DFAILS \leq 0.1$
EFS	Effective failure strain	EFS = 0
TFAIL	Time step size criteria for element deletion	Must be very small but nonzero
ALPH	Shear stress non-linear term	$1E-3 \leq ALPH \leq 1$
SOFT	Crush front strength reducing parameter	Must be calibrated by trial and error
FBRT	Softening factor for fiber tensile strength after matrix failure	$0 \leq FBRT \leq 1$
YCFAC	Softening factor for fiber compressive strength after matrix failure	$0 \leq YCFAC \leq (XC/YC)$
BETA	Weighing factor for shear term in tensile fiber mode	Any value: $0 \leq BETA \leq 1$
XC	Longitudinal compressive strength	F_1^{cu} , from material properties
XT	Longitudinal tensile strength	F_1^{tu} , from material properties
YC	Transverse compressive strength	F_2^{cu} , from material properties
YT	Transverse tensile strength	F_2^{tu} , from material properties
SC	Shear strength	F_{12}^{tu} , from material properties
CRIT	Failure criterion used (MAT54 Chang-Chang, MAT55 Tsai-Wu)	Assign value of 54 or 55

^{*} For English units, must be divided by a gravity factor to convert from pound-weight to pound-mass.

accommodate small errors in measured strength and stiffness. Yet, it should be sensitive enough to capture more significant variations, which translates in being able to capture different behaviors for different input material properties. The sensitivity of the model to variations in strengths (XT, XC, SC, YT, and YC) and strains-to-failure (DFAILT, DFAILC, DFAILM, DFAILS and EFS) is discussed in this section of the paper.

Varying fiber tensile strength XT above or below the baseline value does not affect the outcome of the simulation, except for extreme cases where $XT \leq 5$ ksi (34.47 MPa), which is not physically meaningful. This observation seems to suggest that fiber tension strength is not a primary failure driver for the given specimen geometry-material combination.

On the other hand, varying fiber compressive strength XC has a great effect on the resulting load–displacement curve. Small increments in XC (making it less negative) significantly lower the average crush load, while small decreases of XC (making it more negative) significantly raise the average crush load, at least until a stability threshold is reached and the model becomes unstable, Fig. 8. This instability occurs at $XC = -275$ ksi (-1896 MPa). The model’s strong dependence on XC would suggest that the dominant failure mode occurring during these crush simulations is the compressive fiber mode.

Shear strength SC has an unexpectedly strong and peculiar influence on the stability of the model. Increasing SC above the baseline value does not affect the results, even up to values that are twice the experimental strength of the material. On the other hand, decreasing SC by even small amounts (approximately 15% of the experimentally measured value) creates instabilities in the model, Fig. 9. Increasingly lower values of SC cause greater instabilities in the crush curve. Interestingly, MAT54 does not have a failure criterion dedicated to shear strength, but SC appears as an interactive term in Eqs. (4), (6), and (7) in the tensile fiber (through the parameter BETA if nonzero), tensile matrix, and compressive matrix failure modes. By decreasing SC, the contribution due to the shear term in the three equations increases, combining with the other stress, to the point that it causes premature ply and element failure. The results indicate that shear strength is a fundamental parameter for the stability of the specimen during crushing, and that particular care should be placed in determining the correct experimental value. The difference that exists between the baseline (22.4 ksi or 154.4 MPa) and the partially unstable simulation (19 ksi or 131 MPa) is within experimental error, particularly for a difficult test such as the one for shear strength.

Varying the matrix tensile strength YT, which is found in the failure criteria for the tensile matrix mode only (Eq. (6)), in the range from 0 to 300 ksi (2068 MPa), with the baseline value being 7.09 ksi (48.9 MPa), does not affect the results: the load–displacement curve remains stable and the average crush load does not change.

Varying the matrix compressive strength YC, found in the failure criteria for the compressive matrix mode only (Eq. (7)), does not change the results of the crush simulation. However, for exceptionally high values, such as 200 ksi (1379 MPa), the crush curve is approximately 10% lower than the baseline curve. Since this value is not realistic for unidirectional tape, it can be neglected. Matrix (2-direction) tension and compression are therefore not failure driving mechanisms for this geometry/material combination under crush loading.

For the tensile strain-to-failure in the fiber direction, DFAILT, the simulation results remain unchanged from the baseline, which uses a nominal value of +0.0174, and a range from a high of +0.070 to a low of +0.0075. This finding suggests that allowing for a virtual plasticity [16] in the positive direction does not affect the simulation, Fig. 10. However, if the strain-to-failure is further reduced, below +0.0075, instabilities start to manifest, with non-uniform

Table 3

MAT54 baseline model input deck (strikethrough values are not used).

*MAT_054 (ENHANCED_COMPOSITE_DAMAGE)							
mid	ro	ea	eb	(ee)	prba	(prea)	(preb)
1	.1500E-3	.1840E+8	1220000	0.0	0.02049	0.0	0.0
gab	gbc	gca	(kf)	aopt	a1	a2	a3
610000.0	610000.0	610000.0	0.0	3.000	0.0	0.0	0.0
mangle	v1	v2	v3	d1	d2	d3	
90.000	0.0	0.0	1.000	0.0	0.0	0.0	
dfailm	dfails	dfailt	dfailc	efs	tfail		
0.02400	0.03000	0.01740	-0.01160	0.0	.11530E-8		
alph	soft	fbrt	ycfac	beta			
0.10000	0.57000	0.50000	1.200	0.50000			
xc	xt	yc	yt	sc	crit		
-213000.0	319000.0	-28800.00	7090.000	22400.00	54.000		

Table 4

Summary of the parametric studies performed (units not shown for clarity).

Parameter	Baseline value	Parametric variation	Figure
MAT54: XT	319,000	0, 5000, 50,000, 150,000, 250,000, 300,000, 350,000, 370,000, 400,000, 500,000, 640,000	–
MAT54: XC	-213,000	0, -100,000, -150,000, -200,000, -230,000, -250,000, -265,000, -275,000, -300,000	8
MAT54: SC	22,400	1, 10,000, 15,000, 175,000, 18,000, 19,000, 20,000, 30,000, 35,000, 50,000	9
MAT54: YT	7090	0, 3000, 6800, 7500, 10,000, 50,000, 500,000	–
MAT54: YC	-28,800	0, -5000, -15,000, -25,000, -30,000, -35,000, -70,000, -200,000, -288,000, -320,000, -400,000, -500,000	–
MAT54: DFAILT	0.0174	0, 0.005, 0.00625, 0.00688, 0.0075, 0.01, 0.015, 0.04, 0.08	10
MAT54: DFAILC	-0.0116	0, -0.005, -0.0075, -0.00813, -0.00875, -0.01, -0.012, -0.015, -0.02, -0.0225, -0.025, -0.03, -0.1	11
MAT54: DFAILM	0.024	0, 0.01, 0.015, 0.0163, 0.0165, 0.018, 0.02, 0.03, 0.06	12
MAT54: DFAILS	0.03	0, 0.006, 0.01, 0.037, 0.05, 0.1	–
MAT54: EFS	0	0.01, 0.5, 1	–
MAT54: ALPH	0.3	0, 1.00E-14, 1.00E-6, 1.00E-4, 1.00E-3, 0.03, 0.9, 1	–
MAT54: BETA	0.5	0, 1	–
MAT54: FBRT	0.5	0, 0.1, 0.95, 1	–
MAT54: YCFAC	1.2	0, 0.5, 2, 4, 7.396, 9	–
MAT54: TFAIL	0.115E-08	0, 1E-07, 0.05, 0.11	–
MAT54: SOFT	0.57	-0.5, 0, 0.05, 0.4, 0.55, 0.565, 0.575, 0.6, 0.8, 2	13
SAE filter frequency	600	180, 1000	14
Crush speed	150	1.5, 15, 50	15
Contact load–penetration curve	PCWL	PCWL Stiff, PCWL Soft, Linear	16–19
Mesh size	0.1	0.05, 0.15, 0.2	20, 21
Trigger thickness	0.01	0.005, 0.015, 0.020, 0.025, 0.030, 0.035, 0.040, 0.045, 0.047, 0.050, 0.060, 0.079	22
Trigger geometry	Constant thickness	Tapered thickness	23

element failure at both ends of the specimen. For values as low as +0.005, immediate buckling occurs without any stable crushing. This observation seems to suggest that fiber tension strain-to-failure is not a primary failure mode for the given specimen geometry-material combination, as long as the strain-to-failure is sufficiently large to inhibit secondary failures.

The compressive strain-to-failure in the fiber direction, DFAILC, has a more profound effect on the results of the simulation. Within the range [-0.2, -0.0081], around the baseline value of -0.0116, changing DFAILC changes the average crushing load, Fig. 11. Reducing DFAILC (making it more negative) increases the average crush load, while increasing DFAILC (making it less negative) decreases the average load value. Lowering DFAILC below -0.02 however leads to non-uniform element deletion at the crush front, Fig. 11. Adding virtual plasticity [16] has a detrimental effect on the simulation results. On the other hand, if DFAILC is increased up to -0.0081, global buckling occurs immediately. Based on these results, compressive strain-to-failure is a primary failure mode for the given specimen geometry-material combination, and therefore a critical parameter for achieving successful simulation results.

In the transverse direction, the positive and negative failure strains are both defined by a single parameter, DFAILM. Since from experiment the compressive strength of the matrix is greater than its tensile strength (Table 1), it is not easy to define a single strain-to-failure value for both directions using only one parameter, Fig. 4b. As such, this challenge constitutes a clear limitation of the MAT54 material model. For the baseline model, DFAILM is set to be the compressive strain-to-failure [0.0240], which automatically imposes a plateau of “virtual plasticity” in tension, Fig. 4b. Adding more “plasticity” by increasing DFAILM to values as high as [0.100] does not affect the simulation. On the other hand, decreasing DFAILM beyond the critical value of [0.0165] eventually leads to global instabilities, with non-uniform element deletion and large load fluctuations, Fig. 12. In the extreme, setting DFAILM to zero causes severe element distortion, element detachment without deletion, and non-uniform deletion. The results therefore indicate that DFAILM is a fundamental parameter for the stability of the simulation.

From the baseline value of DFAILS = 0.03, the shear strain-to-failure is varied in the range [0, 0.10]. It is found that the crush

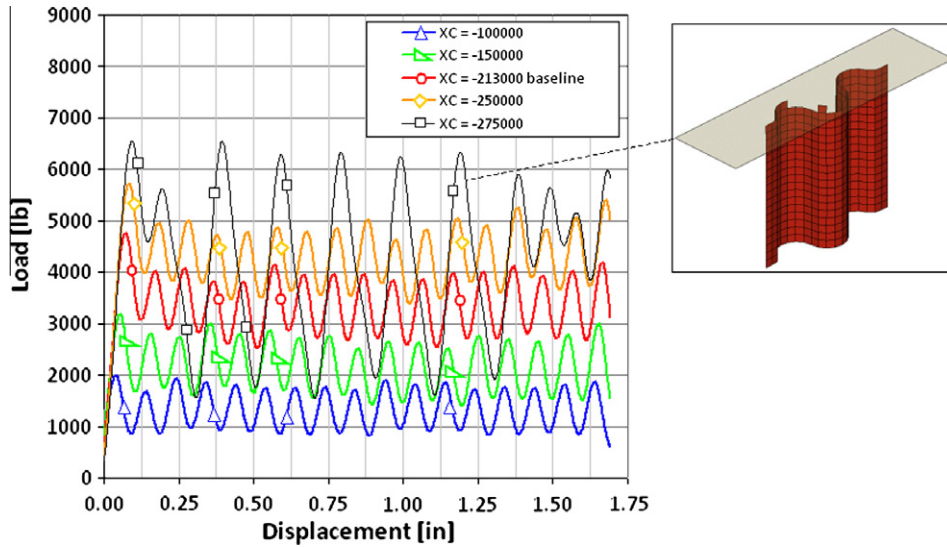


Fig. 8. Effect of varying compression strength XC on the baseline model, showing that small changes to XC lead to large changes in the simulation results. (For interpretation of the references to colour in this figure legend, the reader is referred to the web version of this article.)

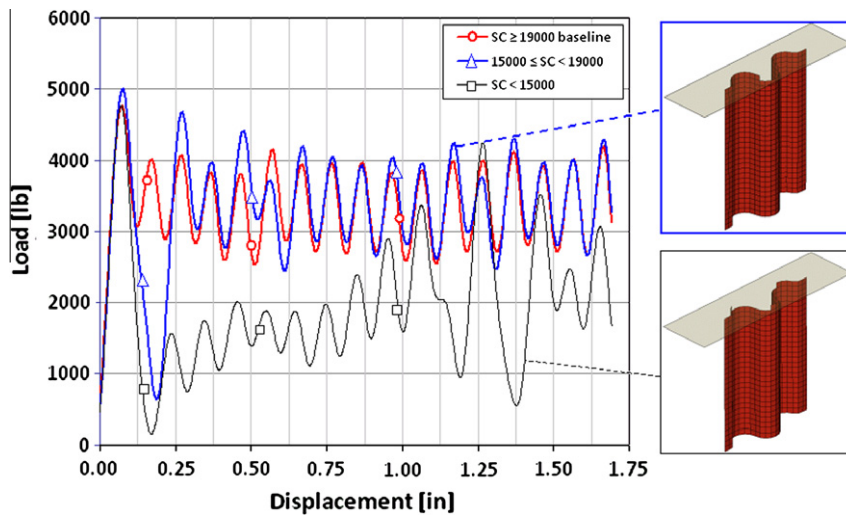


Fig. 9. Effect of varying shear strength SC on the baseline model, showing an unexpected influence of shear strength on the stability of the model. (For interpretation of the references to colour in this figure legend, the reader is referred to the web version of this article.)

load–displacement curve remains unaltered from the baseline, thus suggesting that either shear is not a dominant failure mechanism for this crush problem, or that the model is not able to capture shear-related phenomena. While MAT54 allows the element to fail if the strain exceeds DFAILT, DFAILC or DFAILM, it should be noted that there is no explicit criterion for failure associated with DFAILS.

The EFS parameter is a measure of a general strain-to-failure in the absence of the individual values of DFAILT, DFAILC, and DFAILM. If these values are defined, the model neglects the value of EFS, and it is found that indeed altering the EFS between [0, 1] does not change the simulation results at all. However, if DFAILT, DFAILC and DFAILM are set to zero and EFS is utilized, the model encounters errors and does not run at all for any value of EFS. Therefore, for this type of crush simulation, it is recommended to always utilize the experimentally measured strains to failure for the unidirectional lamina and not rely on an arbitrary value of EFS.

From these results, it appears that compressive strength XC and compressive strain-to-failure DFAILC are the dominant parameters

controlling element failure, and therefore have a strong influence on the predicted load–displacement results.

6. Sensitivity of the MAT54 material model to other model-specific parameters

This section focuses on the effect of parameters that are specific to the MAT54 material model, and that are necessary for the simulation to progress in a stable fashion. These parameters either have no immediate significance in the physical world or cannot be measured experimentally, and hence have to be calibrated by trial and error. These quantities include the ALPH, BETA, FBRT, YCFAC, SOFT and TFAIL parameters, as summarized in Table 1.

The ALPH and BETA parameters, which appear in Eqs. (3) and (4) respectively, are shear stress weighing factors that may hold values between [0, 1]. Parametric studies reveal that using any value of ALPH or BETA in the admissible range does not influence in any way the baseline simulation, both in terms of

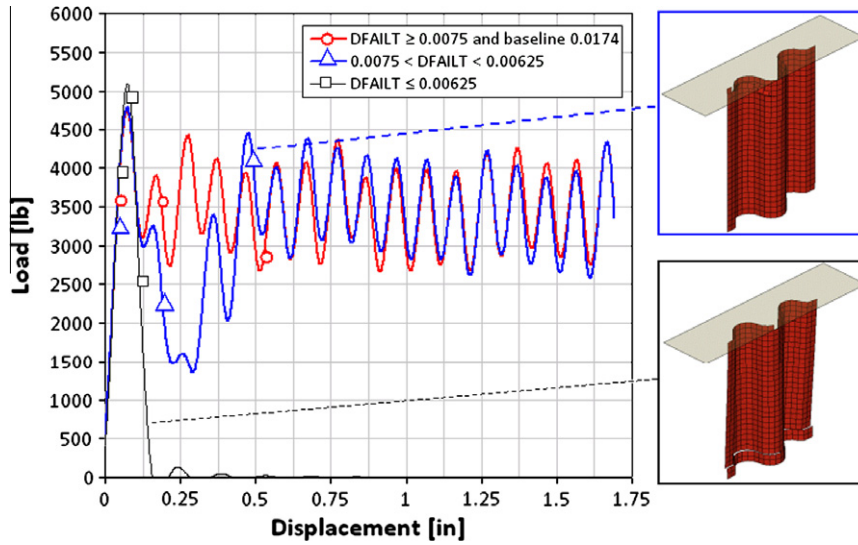


Fig. 10. Effect of varying tension strain-to-failure DFAILT; only very low values of DFAILT lead to non-uniform element deletion (unstable crushing) and global buckling (failure at the other end of the specimen). (For interpretation of the references to colour in this figure legend, the reader is referred to the web version of this article.)

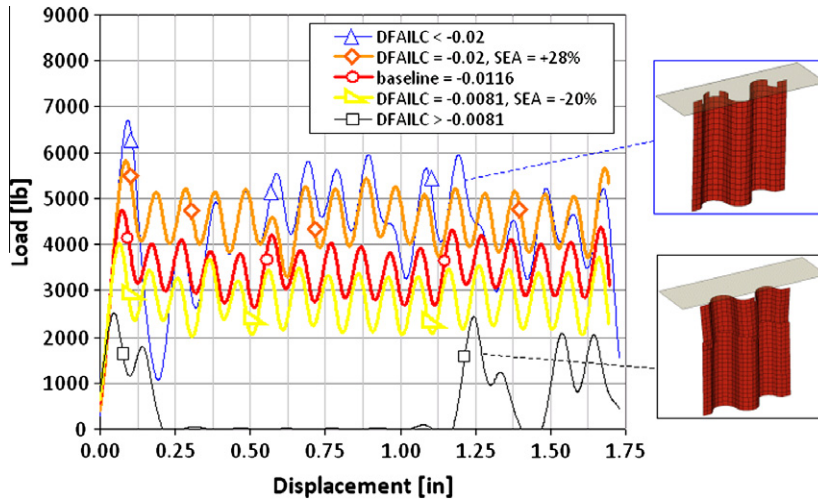


Fig. 11. Effect of varying compression strain-to-failure DFAILC, showing that small changes to DFAILC have dramatic influence on the simulation results. (For interpretation of the references to colour in this figure legend, the reader is referred to the web version of this article.)

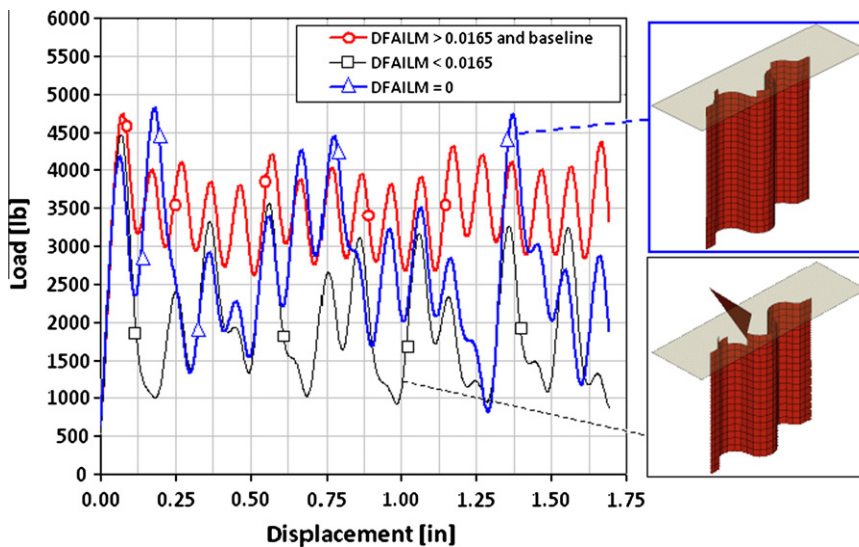


Fig. 12. Effect of varying matrix strain-to-failure DFAILM, showing that DFAILM has a significant role in the stability of the simulation. (For interpretation of the references to colour in this figure legend, the reader is referred to the web version of this article.)

load–displacement curve and SEA. The independence of the BETA term suggests that shear stress has no effect on fiber failure, which in turn signifies that the failure criterion used for tensile fiber failure (Eq. (4)), whether Hashin (BETA = 1) or Maximum Stress (BETA = 0), is not critical to the outcome of the simulation. This observation, in conjunction with the previous observations for XT and DFAILT, seems to confirm that fiber tension failure is not a primary damage mechanism. On the other hand, the insensitive nature of this model to the value of the ALPH parameter, which adds the third-order shear term in Eq. (3), seems to suggest that the shear stress–strain relation can be simplified to a first-order equation for this material/geometry/loading combination.

The strength reduction factors FBRT and YCFAC were arbitrarily selected to be equal to 0.5 and 1.2 respectively for the baseline simulation (Table 2). Both the FBRT and YCFAC terms are fiber strength reduction factors (for XT and XC respectively) for elements that have already experienced damage. They are used to degrade the fiber strength properties of the element following the first-ply (matrix) failure. These properties are varied systematically in the range [0, 1] for FBRT and [0, 7.4] for YCFAC. Results show that the simulation is unaffected by the fiber strength degradation scheme. These factors have negligible effect on the results of the simulation.

As for TFAIL, the simulation results were unaffected for small values of TFAIL, such as [1E-08, 1E-05]. Using TFAIL = 0 leads to immediate global buckling because of the SOFT condition violation discussed earlier. Using large TFAIL values in the range [0.001, 0.1] should be avoided, since the time-step of the simulation is smaller and elements are deleted before being loaded. It should be emphasized that LS-DYNA assigns the time-step automatically to ensure that the Courant condition is satisfied [17–19]. In this case the default time-step is 2.44219 E-7 [6].

The sensitivity of the model to variations in the SOFT parameter is investigated within the admissible range [0, 1]. Values above 1.0 are confirmed to yield the same curve as if SOFT were set to 0. For values above 0 but less than 1.0, results show that SOFT has a dramatic effect on the simulation and is perhaps the single most influential parameter in the entire input deck, Fig. 13. By itself, it is capable of dictating whether the simulation is stable or unstable. It can also shift the average crush load above or below the baseline by at least 30% from the baseline value of 64.12 J/g (for SOFT = 0.57). The results are shown in Fig. 13, along with the average SEA values. Increasing the SOFT value has the effect of increasing the average crush load and SEA of the simulation. For SOFT = 0.6, SEA = 75.8 J/g (+13%), for SOFT = 0.8, SEA = 87.1 J/g (+30%) and partial instability occurs halfway in the simulation.

Further increasing the SOFT parameter to 0.95 makes the specimen too stiff and it buckles immediately. Lowering the SOFT parameter has the effect of lowering the average crush load and SEA value of the simulation. For SOFT = 0.4, SEA = 48.8 J/g (–27%), and it could go even lower for lower values of the SOFT parameter (for SOFT = 0.05, SEA = 2.74 J/g or –96%). It should be recalled that the meaning of the SOFT parameter is to artificially reduce the strength of the row of elements immediately ahead of the active crush front. This parameter is a mathematical expedient to avoid global buckling of the specimen, which would occur if the peak load were transferred instantaneously upon deletion from the active crush front to the row of elements immediately ahead of the crush front. The transfer of loading between element rows is responsible for the jagged peak–valley behavior of the unfiltered load–displacement curve of Fig. 6. In the physical world one could interpret the SOFT parameter as a damage zone (comprised of delaminations and cracks) ahead of the crush front that reduces the strength of the material. When that material undergoes crushing, it has strength lower than its pristine value. Determining the correct value of the SOFT parameter is a challenging task, since it cannot be measured experimentally, but it has to be found by trial and error until the load–displacement curve of the simulation matches the experimental result. Unless the right value of the SOFT parameter is found and utilized, it is not possible to obtain a successful simulation. The most important consequence of this observation is that the MAT54 material model is not a true predictive tool since the SOFT parameter needs to be calibrated to the experiment.

7. Sensitivity of the model to other modeling parameters

In this section, the influence of parameters that are not specific to the material model itself but are particularly influential for the execution of the simulation is discussed. These include filtering, crush speed, load–penetration (LP) curve, mesh size, trigger thickness and trigger shape.

The choice of frequency for the filter can significantly change the behavior of the crush curve. Low-pass filter frequencies are useful to damp large variations in load, however they can also mask out important physical information such as the initial slope and peak load. It is desirable to use a frequency that is high enough to capture the initial slope and peak, while sufficiently attenuating (smoothing) the load–displacement curve. Typically, the correct low-pass filtering frequency is determined by measuring the duration of the acceleration pulse from accelerometer data recorded during impact. Since this data is not available for the coupon level test, frequencies from the Channel Frequency Class (CFC) for

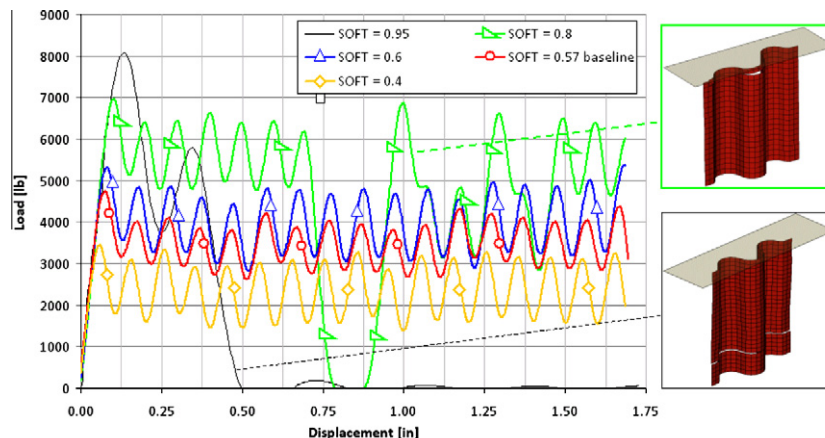


Fig. 13. Effect of the SOFT parameter on the simulated load–displacement curve shows that this parameter is the single-most critical and influential parameter for the results of the simulation. (For interpretation of the references to colour in this figure legend, the reader is referred to the web version of this article.)

vehicle impact are investigated to find the appropriate filtering frequency. Varying the CFC frequencies of 180 and 1000 Hz from the baseline value of 600 Hz produces the curves shown in Fig. 14. The 600 Hz filter has the lowest frequency which maintains the initial slope of the curve, and for this reason is the most commonly used filter in crash analysis [15]. Using a 180 Hz frequency filter causes loss of both the initial slope and load peak, while the 1000 Hz filter retains large load peaks that mask the initial physical peak and the stable crush load. The resulting SEA value changes only a few percent, but the overall load–displacement curve loses significance. A known effect associated with filtering, regardless of the frequency used, is the shift of the load–displacement curve to the left, causing the initial load in the filtered curve to be non-zero. This phenomenon, which is purely mathematical and not physical, can be seen dramatically in Fig. 14 for the 600 and 180 Hz filters. Filtering causes an initial load at time zero to be close to 2000 lb (8.896 kN) using these filters.

Although the true experimental crush loading rate is 1.0 in./min. (25.4 mm/min), simulations are performed using a crush velocity of 150 in./s (3810 mm/s) because of computational runtime limitations. Since all material properties were measured with quasi-static tests, no strain-rate dependent material properties were defined in the input deck (material card), hence the model cannot assume strain-rate behavior. Nonetheless, inertial effects may arise, which could lead to different global response for the specimen. To verify the validity of the assumption, two simulations are carried out at simulation speeds of 15 in./s (381 mm/s) and 1.5 in./s (38.1 mm/s), which are both well below any dynamic threshold reported in the literature [1,2,5]. These simulations have runtimes of 16 min and 164 min respectively, compared to the runtime of 96 s of the baseline model, and are hence very impractical with the available computational power. Reduced crush speeds do not change significantly the results from the baseline simulation, Fig. 15.

Varying the LP curve has an important effect on the stability of the model, yet there is no way of knowing *a priori* or determining experimentally what correct shape this curve needs to have for the specific material/geometry/loading combination. Definition of the LP curve takes place by trial and error. The baseline LP curve is a piecewise linear (PCWL) function, Fig. 16, which introduces the load in a gradual fashion into the coupon. If the stiffness of the PCWL function is varied above and below that of the baseline, the LP curves take the shapes shown in Fig. 16 (stiff and soft respectively). A stiff LP curve introduces the load into the coupon more suddenly, while a soft LP curve introduces the load more

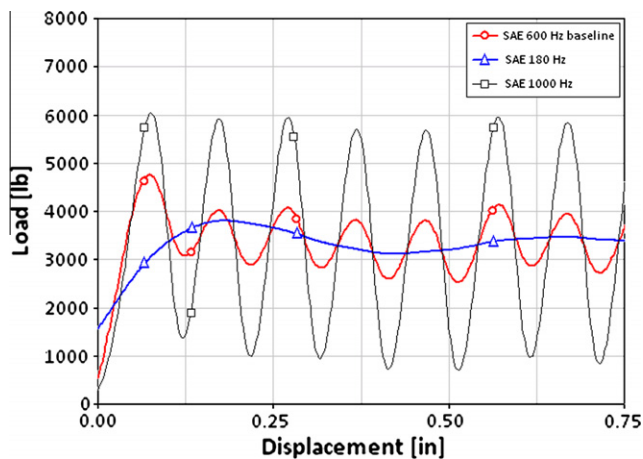


Fig. 14. Effect of SAE filter frequency on the baseline simulation. (For interpretation of the references to colour in this figure legend, the reader is referred to the web version of this article.)

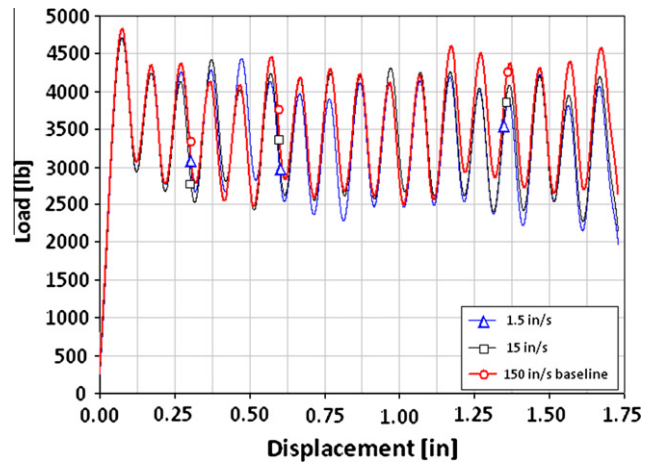


Fig. 15. Effect of crush velocity on the simulation results: quasi-static speeds cannot be executed efficiently because of computational limitations, but trends suggest that minor differences in results should be expected. (For interpretation of the references to colour in this figure legend, the reader is referred to the web version of this article.)

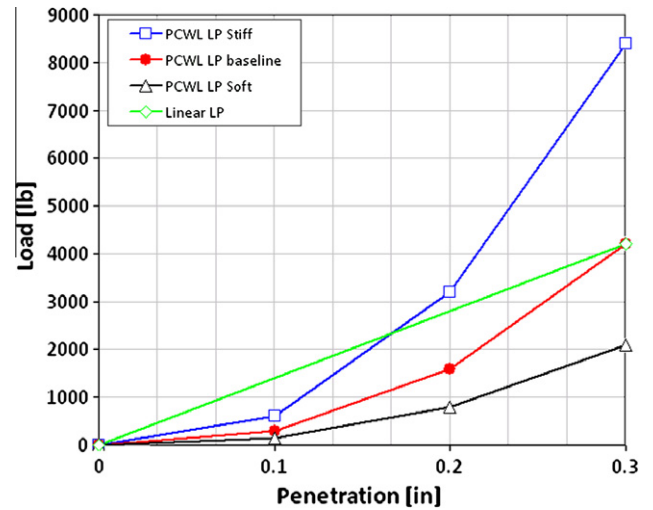


Fig. 16. Four different load–penetration curves investigated in the contact definition. (For interpretation of the references to colour in this figure legend, the reader is referred to the web version of this article.)

gradually. It should be expected that using a stiff LP curve would increase the reaction forces on the elements, which in turn would increase the slope of the load–displacement curve (i.e. the load increases faster to its plateau) and the magnitude of the peak load oscillations, thus raising the average crush force. The opposite should be expected for a soft LP curve. Filtered results show that the stiff LP curve leads to a greater stiffness as expected, but lower peak load and lower average crush load, while the soft LP curve generates lower initial stiffness, but higher peak load and average crush load than the baseline (Fig. 17). This counterintuitive result is however only a deception of the analysis due to the filtering scheme. If the raw load–displacement curves for the baseline and stiff LP curves are plotted (Fig. 18 shows only these for clarity), it can be seen that indeed the stiff LP curve generates higher peak loads than the baseline curve. Increasing the LP curve also leads to element failure and deletion well before the loading plate reaches the next row of elements. This behavior results in greater positive/negative oscillations and long periods where zero-load exists before the next row of elements contacts the plate. The higher

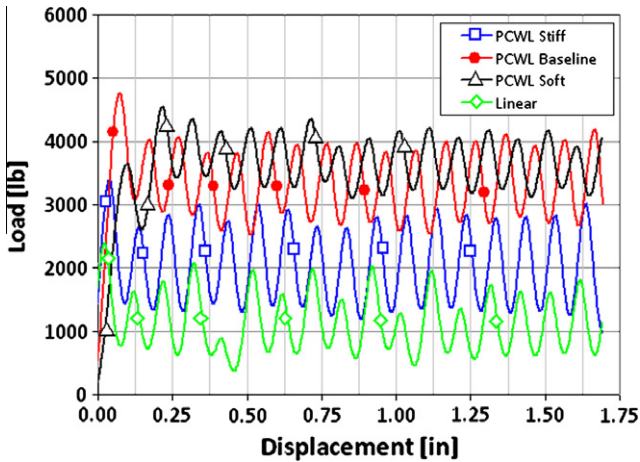


Fig. 17. Effect of the four different load–penetration curves (from Fig. 16) on the filtered load–displacement curves. (For interpretation of the references to colour in this figure legend, the reader is referred to the web version of this article.)

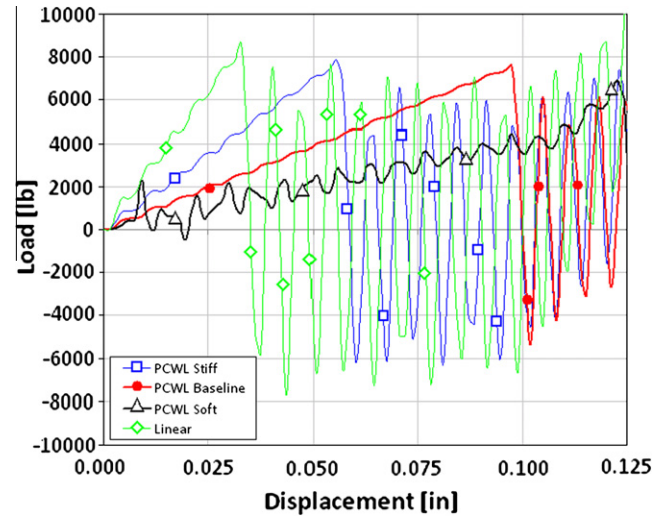


Fig. 19. Details of the influence of the four load–penetration curves on the initial time-steps of the four different raw (unfiltered) load–penetration curves. (For interpretation of the references to colour in this figure legend, the reader is referred to the web version of this article.)

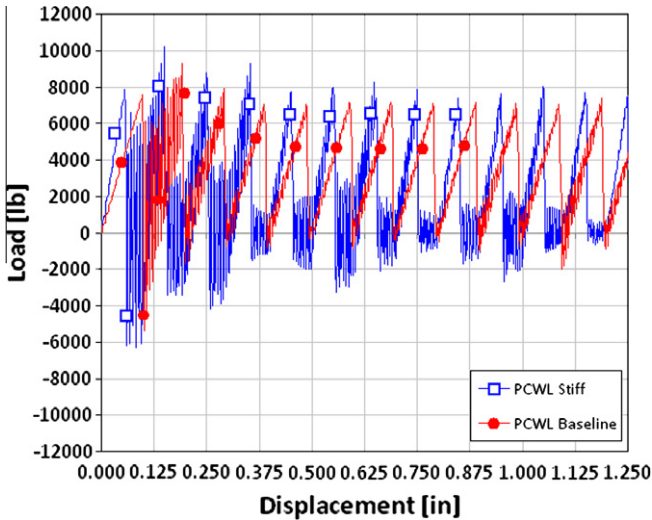


Fig. 18. Two raw (unfiltered) load–displacement curves from Fig. 17. (For interpretation of the references to colour in this figure legend, the reader is referred to the web version of this article.)

oscillations and zero load regions in between element rows decrease the average crush load as calculated by the SAE filter. In the extreme, if an aggressive linear LP curve is used (Fig. 16), which leads to the same final load value as the PCWL LP curve of the baseline but at a much faster rate, the filtered load–displacement curve shows a higher initial stiffness but an even lower average crush load than the stiff PCWL LP curve, Fig. 17. The raw load–displacement curves for all four types of LP curves are shown in Fig. 19, where for clarity only the early portion of the curve is reported. It can be seen that the linear LP curve has the highest initial stiffness and the most variation between positive and negative amplitudes, while the soft PCWL LP curve leads to the lowest initial stiffness and most moderate oscillations. Using a softer LP curve leads to lower peak values, which in turn leads to element deletion only when the next row of element is already contacting the plate. Thus the load never drops to zero, and the SAE filter provides a higher average crush load.

Explicit FEA codes are known to be particularly mesh-sensitive, and while it is desirable to always use the finest mesh size, computational costs become particularly demanding. From the baseline

value of 0.1 in. (2.54 mm), the mesh size is varied down to 0.05 in. and up to 0.2 in. (1.27 mm and 5.08 mm respectively). All other parameters are left unchanged from the baseline model. While the runtime for the baseline mesh size is 96 s, the run times for the finer mesh is 7 min 19 s, while for the coarser mesh it is 43 s. The filtered load–displacement curve for the coarse mesh, Fig. 20, shows that the initial load and slope are very close to the baseline, but the curve never achieves a stable crush load. The filtered curve oscillates with greater amplitude than the baseline, and the reason for this behavior can be found by looking at the raw curve. Once a row of elements fail, there is a large gap with zero load before the next row of elements comes into contact with the loading plate, similarly to the case of the stiff LP curve. Intuitively, softening the LP curve would correct this behavior, however trials show that sustained crushing without zero loading cannot be achieved no matter how soft the LP curve is. Softening the LP curve also reduces the initial peak load and slope, and the average crush load is overall lower than the baseline due to the presence of the zero-load sections. Attempts to raise the curve have been made by increasing the SOFT parameter, which increases the peak loads, however it is not sufficient to increase the average crush load to an acceptable value. The coarse mesh size appears to be too coarse to capture the relevant behaviors. Another observation that supports this conclusion is that the element formulation 16 in LS-DYNA is a linear shell element, and therefore it cannot be curved or bent to conform to a curved geometry. For the sinusoid specimen, characterized by continuous curvature with a radius of 0.25 in. (6.4 mm), the coarse mesh approximates the sinusoid geometry too roughly, Fig. 20 right. Quadratic shell elements are not currently available in LS-DYNA [6]. The finer mesh yields the load–displacement curve of Fig. 21. Without changing any other parameters, the load has a larger initial slope and peak value, which is followed by instability and large oscillations, and eventually undergoes global buckling. In this case, by reducing the SOFT parameter (from 0.57 to 0.50), the finer mesh simulation achieves sustained crushing, with only minor instability at the beginning of the simulation, as seen in the stable crush curve of Fig. 21. Attempts to stabilize the model by modifying the LP curve yield even more unstable results. The oscillations for the modified fine-mesh model have higher frequency and amplitude as a result of the doubled number of element rows, but overall the finer mesh model matches the experimental data well.

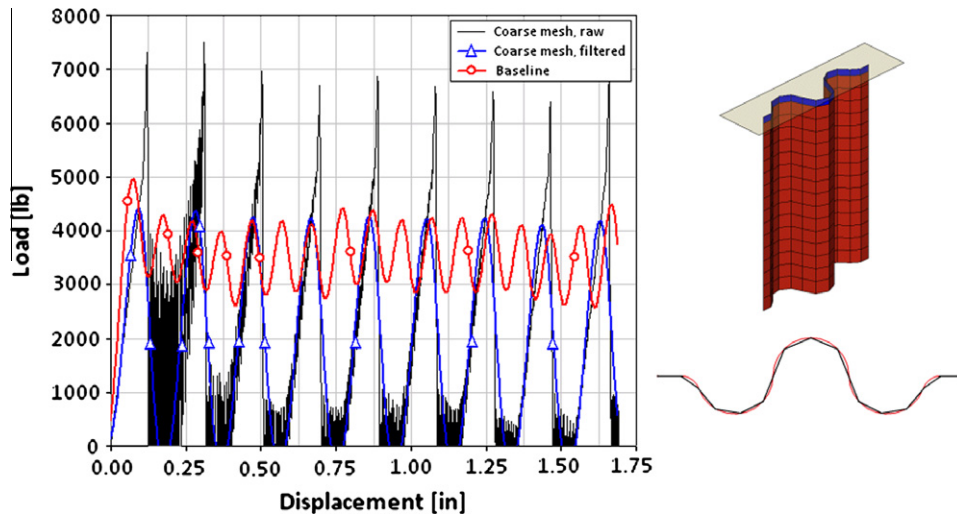


Fig. 20. Effect of coarser mesh size on the baseline load–displacement curve, both filtered and raw (unfiltered). (For interpretation of the references to colour in this figure legend, the reader is referred to the web version of this article.)

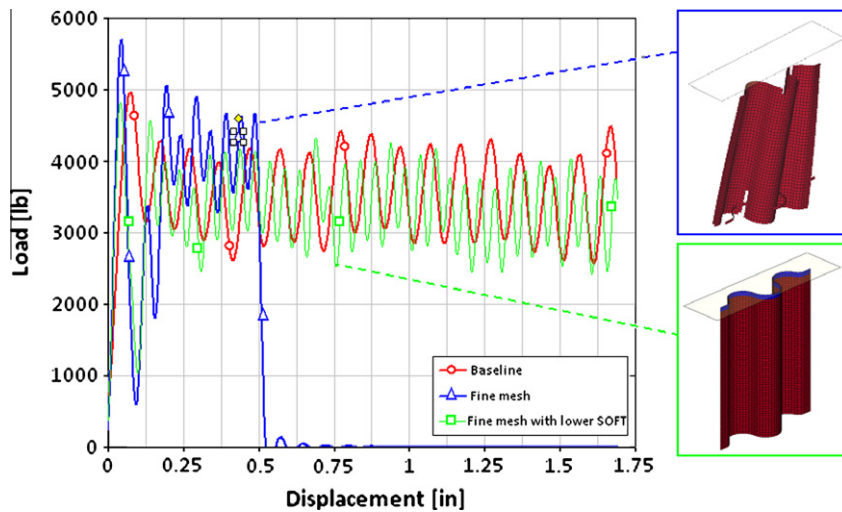


Fig. 21. Effect of finer mesh size on the baseline filtered load–displacement curve, with baseline and reduced SOFT parameter. (For interpretation of the references to colour in this figure legend, the reader is referred to the web version of this article.)

The crush trigger determines the initial behavior of crushing, directly influences the initial peak load value, and can also influence crush stability. The baseline trigger geometry is a single row of constant reduced thickness elements (0.01 in. or 0.25 mm). The thickness is varied between 0.001 and 0.5 in. (0.025 mm and 12.7 mm) and it is found that increasing trigger thickness up to a thickness of 0.047 in. (1.19 mm) leads to lower initial peak load than thinner triggers, Fig. 22. However, similar to the previous discussion regarding the LP curve, this behavior is an apparent phenomenon associated with filtering. The raw data shows that early instabilities during crushing can cause the second row of elements to be deleted simultaneously with the trigger row, leading to near zero load, which the filter then interprets as a lower initial peak load. Increasing the thickness to 0.05 in. and above (12.7 mm) leads to immediate global instability, which causes the specimen to buckle, Fig. 22. Since the trigger is at the contact interface of the loading plate, the choice of contact formulation affects the sensitivity of the trigger thickness to the simulation results. For the Entity contact, a thin trigger row of elements is capable of initiating stable crushing and produces the best results for the crush simulation. An alternate trigger geometry is investi-

gated, consisting of a single row of elements having tapered thickness, which varies linearly from 0 to 0.079 in. (2 mm, the full thickness of the specimen). This trigger more closely resembles the geometry of the physical trigger. The tapered trigger has a slightly lower initial peak load than the constant-thickness trigger, however the global response and average crush load are nearly identical, Fig. 23.

From the sensitivity studies performed, it becomes clear that there may be more than one way to obtain a “baseline” simulation. Mesh size and contact formulation have a dramatic effect on the simulation, and it is possible to adjust these parameters to obtain multiple baselines. Furthermore, for a given mesh size and contact formulation, it is possible to obtain a good match to the experimental data using multiple combinations of MAT54 parameters, in particular the SOFT parameter, XC and DFAILC, which have the most influence on the simulation results. The combinations of these parameters for five equivalent baseline simulations are summarized in Table 5. If DFAILC is reduced from the baseline value, the load–displacement curve tends to exhibit higher average crush load, Fig. 11. However, if the SOFT parameter is reduced, the load–displacement curve tends to exhibit lower average crush

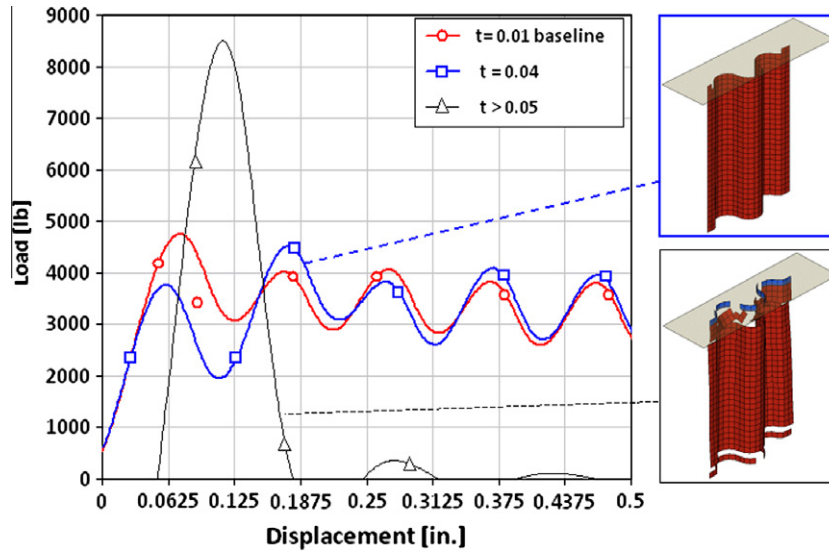


Fig. 22. The thickness of the baseline trigger (which is a single row of elements of reduced constant thickness) has a crucial effect on the initial peak and the stability of the load–displacement curve. (For interpretation of the references to colour in this figure legend, the reader is referred to the web version of this article.)

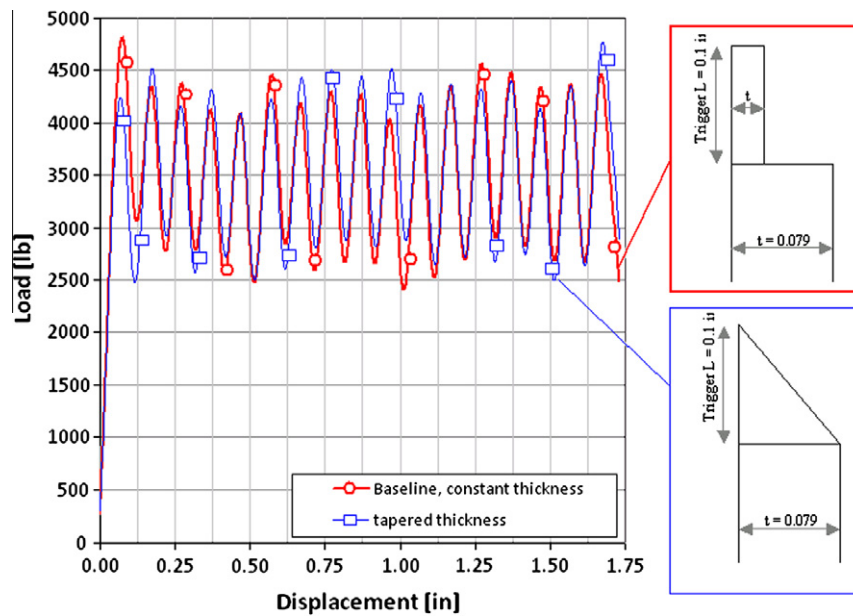


Fig. 23. Very similar results can be used with two different trigger geometries, one of reduced constant thickness (baseline) and one with tapered thickness (similar to the physical trigger). (For interpretation of the references to colour in this figure legend, the reader is referred to the web version of this article.)

Table 5
Summary of the numeric baselines.

Baseline	Contact type	LP curve	Mesh size	SOFT	DFAILC	XC	SEA (J/g)	% Error
1	Entity	PCWL baseline	0.1	0.57	−0.0116	−213,000	64.12	−4.4
2				0.48	−0.0175	−213,000	67.32	+0.4
3				0.615	−0.0100	−213,000	67.80	+1.1
4				0.62	−0.0116	−200,000	66.39	−1.0
5				0.54	−0.0116	−230,000	66.49	−0.9

load, Fig. 13. If both are varied at the same time, the two effects counteract each other and the resulting load–displacement (baseline 2 in Fig. 24) curve matches the experimental one as well as the original baseline 1 (Table 5). Similarly, if DFAILC and SOFT are simultaneously increased, the resulting load–displacement curve also matches the experimental data, baseline 3 in Fig. 24

and Table 5. Similar trends can be obtained by varying XC and SOFT by a small amount, to obtain nearly identical crush load–displacement curves (baselines 4 and 5). Therefore, DFAILC, XC and SOFT can be adjusted simultaneously to yield multiple combinations that generate accurate results. It is therefore important to ensure that the correct experimental material properties are used, and

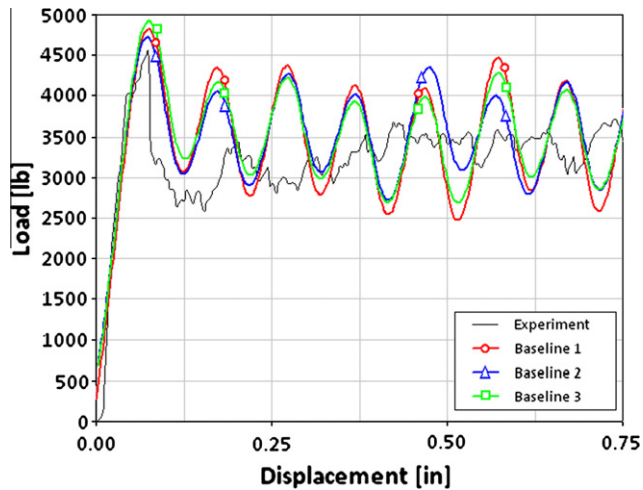


Fig. 24. Multiple baselines (1–3 in Table 5) obtained by varying simultaneously DFAILC and SOFT. (For interpretation of the references to colour in this figure legend, the reader is referred to the web version of this article.)

that the analyst is fully aware of the sensitivity of the model to variations in these parameters.

As a result of this investigation it is possible to summarize some key observations regarding the most fundamental input parameters and their role in this crush simulation. The shape of the LP curve has a dramatic effect on the initial elastic slope of the LD curve. The thickness of the trigger has a dramatic influence on the first failure load, which is also the peak load. DFAILM has a large effect on the overall stability of the model, and can dictate stable or unstable crushing. DFAILC and XC have most influence on the average crush load. The SOFT parameter can by itself regulate the initiation of stable crushing as well as shift up or down the average crush load.

Based on these observations, the proposed modeling approach is considered to be non-predictive for the sinusoidal specimen, since it is not possible to simulate its crushing behavior with a sufficient level of confidence based solely on the material properties derived from tension, compression and shear coupon level tests. For these reasons, the sinusoidal specimen crush test should be interpreted as an element-level test, from which the analysis model can be successfully calibrated. Following the calibration at the element level of structural complexity, it is expected that the simulations will become predictive. At the assembly level (sub-component and full-scale component), the analysis model will be sufficiently robust to be used for validation without further calibration. However, it is imperative that the assembly be comprised of elements having the same geometry as the sinusoidal elements tested. It is expected that if the elements were to exhibit differences in thickness or degree of curvature, even while maintaining material and manufacturing process unchanged, the analysis model will lose its predictive capability, and additional element-level testing and model calibration will need to be performed. Since strength and strain-to-failure parameters are required to remain unchanged (since materials and process are also unchanged), it is expected that the SOFT parameter and possibly trigger or load-penetration curve will need to be tailored *a posteriori* for each geometry considered.

8. Conclusions

Dynamic failure analysis, such as the crush model developed in this paper, is a complex effort that requires a deep understanding of the sensitivity of the model to input parameters. LS-DYNA

material model MAT54 can be used to successfully simulate the behavior of a sinusoidal composite specimen undergoing axial crushing. The model exhibits stable and progressive element failure and deletion, and is capable of capturing with accuracy the peak and average crush loads, as well as the overall load–displacement response. Through a sensitivity study, it was shown that the fiber compression strength XC and strain-to-failure DFAILC are the primary material parameters leading to element failure and deletion. The SOFT crush front parameter is the single most influential parameter for determining the success of the simulation. Through a careful calibration by trial-and-error, the appropriate value for the SOFT parameter can be identified, but there is no way of determining it *a priori* or measuring it experimentally. Furthermore, by adjusting the SOFT parameter in conjunction with XC or DFAILC, it is possible to obtain multiple combinations that yield similar simulation results, which match the experimental ones. Other complexities of the model include the selection of the contact definition between the specimen and the crush plate (such as the contact type, load–penetration curve and trigger thickness), mesh size, and filtering scheme. For these reasons, this modeling approach is considered to be not predictive for this level of structural complexity, and requires extensive calibration using the building block approach before conducting the full-scale simulation.

Acknowledgments

The research was performed at the *Automobili Lamborghini* Advanced Composite Structures Laboratory in the Department of Aeronautics & Astronautics, College of Engineering, University of Washington. Funding for this research was provided by the Federal Aviation Administration (Dr. Larry Ilcewicz, Allan Abramowitz, and Curt Davies), The Boeing Company (Dr. Al Miller, Dr. Patrick Stickler, Randy Coggeshall, and Steve Precup), and *Automobili Lamborghini* S.p.A. (Maurizio Reggiani, Luciano DeOto, Attilio Masini). The authors would like to thank Dr. Xinran Xiao (previously at General Motors, now at Michigan State University) for guidance with fundamentals of the explicit finite element modeling.

References

- [1] Carruthers JJ, Kettle AP, Robinson AM. Energy absorption capability and crashworthiness of composite material structures: a review. *Appl Mech Rev* 1998;51:635–49.
- [2] Farley GL, Jones RM. Crushing characteristics of continuous fiber-reinforced composite tubes. *J Compos Mater* 1992;26(1):37–50.
- [3] Hinton MJ, Kaddour AS, Soden PD. A comparison of the predictive capabilities of current failure theories for composite laminates, judged against experimental evidence. *Compos Sci Technol* 2002;62(12–13):1725–97.
- [4] Xiao X. Modeling energy absorption with a damage mechanics based composite material model. *J Compos Mater* 2009;43(5):427–44.
- [5] Feraboli P, Rassaian M. Proceedings of the CMH-17 (MIL-HDBK-17) Crashworthiness Working Group Numerical Round Robin. Costa Mesa, CA, July 2010.
- [6] Hallquist JO. LS-DYNA Theoretical Manual. Livermore Software Technology Corporation; 2005.
- [7] Feraboli P. Development of a corrugated test specimen for composite materials energy absorption. *J Compos Mater* 2008;42(3):229–56.
- [8] Feraboli P. Development of a modified flat plate test and fixture specimen for composite materials crush energy absorption. *J Compos Mater* 2009;43(19):1967–90.
- [9] Feraboli P, Norris C, McLarty D. Design and certification of a composite thin-walled structure for energy absorption. *Int J Vehicle Des* 2007;44(3–4):15–36.
- [10] Tomblin J, Sherraden J, Seneviratne W, Raju KS. A-basis and B-basis Design Allowables for Epoxy-based prepreg Toray T700SC-12K-50C/#2510 Plain Weave Fabric. AGATE-WP3.3-033051-131; September 2002.
- [11] T700SC 12K/2510 Plain Weave Fabric. *Composite Materials Handbook (CMH-17)*, vol. 2. Rev. G. [chapter 4.2.38].
- [12] Browne AL, Johnson NL. Dynamic axial crush of automotive rail sized composite tubes, Part 5: Effect of test conditions. *American Society for Composites (ASC)*. 18th Annual Technical Conference, Paper 152; September 2003, Gainesville, FL.

- [13] Chang FK, Chang KY. A progressive damage model for laminated composites containing stress concentration. *J Compos Mater* 1987;21: 834–55.
- [14] Feraboli P, Deleo F, Wade B, Rassaian M, Higgins M, Byar A, et al. Predictive modeling of an energy-absorbing sandwich structural concept using the building block approach. *Composites (Part A)* 2010;41(6):774–86.
- [15] Fasanella EL, Jackson KE. Best practices for crash modeling simulation. NASA TM-2002-211944, ARL-TR-2849, October 2002.
- [16] Feraboli P, Wade B, Deleo F, Rassaian M. Crush energy absorption of composite channel section specimens. *Composites (Part A)* 2009;40(8):1248–56.
- [17] Paz M. *Structural dynamics theory and computation*. 3rd ed. New York: Van Nostrand Reinhold; 1991.
- [18] Meyer C, Will KM. *Models for dynamic analysis in finite element idealization*. New York: American Society of Civil Engineers; 1987.
- [19] Zukas JA, Nicholas T, Swift HF, Greszczuk LB, Curran DR. *Impact dynamics*. John Wiley & Sons; 1982.